Metals **2015**, *5*, 976-985; doi:10.3390/met5020976

OPEN ACCESS

metals

ISSN 2075-4701

www.mdpi.com/journal/metals/

Communication

Mechanical Behavior of Ultrafine Gradient Grain Structures Produced via Ambient and Cryogenic Surface Mechanical Attrition Treatment in Iron

Heather A. Murdoch *, Kristopher A. Darling, Anthony J. Roberts and Laszlo Kecskes

U.S. Army Research Laboratory, Weapons and Materials Directorate, Aberdeen Proving Ground, MD 21005-5069, USA; E-Mails: kristopher.a.darling.civ@mail.mil (K.A.D.); anthony.j.roberts69.ctr@mail.mil (A.J.R.); laszlo.j.kecskes.civ@mail.mil (L.K.)

* Author to whom correspondence should be addressed; E-Mail: heather.a.murdoch.civ@mail.mil; Tel.: +1-410-306-0699; Fax: +1-410-306-0759.

Academic Editor: Heinz Werner Höppel

Received: 31 March 2015 / Accepted: 21 May 2015 / Published: 3 June 2015

Abstract: Ambient and cryogenic surface mechanical attrition treatments (SMAT) are applied to bcc iron plate. Both processes result in significant surface grain refinement down to the ultrafine-grained regime; the cryogenic treatment results in a 45% greater grain size reduction. However, the refined region is shallower in the cryogenic SMAT process. The tensile ductility of the grain size gradient remains low (<10%), in line with the expected behavior of the refined surface grains. Good tensile ductility in a grain size gradient requires the continuation of the gradient into an undeformed region.

Keywords: grain size gradient; surface mechanical attrition treatment; cryogenic; ultrafine-grained

1. Introduction

Numerous reports now exist indicating an order of magnitude increase in strength is possible in metals and alloys that exhibit grain sizes approaching the lower limit of nanocrystallinity. While achieving high strength has never been a problem, the ability to achieve any amount of uniform elongation (the prerequisite for appreciable ductility) has been a challenge. However, several methods have recently been developed to mitigate this strength-ductility tradeoff through the engineering of multi-length scale structures

including bimodal grain size distributions [1,2], nanoscale twins [3,4], and grain size gradients [5]. Specifically, gradient microstructures generated through surface mechanical attrition treatments or SMAT have additional benefits over other hierarchical microstructures from a surface science/tribological standpoint by concentrating the nanocrystalline properties in the surface region. For instance, nanostructured surface layers have shown improved corrosion resistance [6–9], wear [10,11] and fatigue [12–14], and irradiation resistance [15].

Current SMAT techniques have shown to be very efficient methods for producing grain size gradients, inducing substantial surface grain refinement and varying depths and grades of grain refinement. It has been shown that differences in processing methods can greatly affect both the overall structures (e.g., depth of refined region and "slope" of the grain size gradient) and the individual microstructures (e.g., surface grain size [16], deformation artifacts within grain size regions [16,17]). It was noted by Tao *et al*. [17] in their work introducing SMAT that finer grains would be expected with plastic deformation at lower temperatures. Indeed, Darling *et al*. provided the first evidence in a brief report for this effect through a cryogenic SMAT process on copper [16]. The percent reduction in grain size (60%) due to cryogenic processing is in good agreement with the empirical correlation between the resulting grain size and the Zener-Holloman parameter (combined metric of strain rate and deformation temperature) [18]. In a magnesium alloy, a different surface treatment method resulted in a 63% decrease in grain size for cryogenic burnishing *versus* ambient [19].

As compared to copper, bcc iron would be expected to have a lesser reduction in grain size based on this empirical parameter in addition to the differences in plastic deformation behavior; nanocrystalline/ultrafine-grained iron exhibits essentially no strain hardening [20,21] and an inverse relationship with strain rate sensitivity as compared to fcc materials [21]—especially important as the strain rates involved in the SMAT process are relatively high (~10^2). The cryogenic SMAT process will also take the iron well below its ductile to brittle transition temperature. In this work, we look at the effects of cryogenic and ambient SMAT processing on the microstructure and mechanical properties of iron.

2. Experimental Section

The SMAT process was applied to 0.6 cm thick discs 6.35 cm in diameter cut from a rod of ARMCO iron (Goodfellow, Huntington, UK; purity > 99.85%Fe). Details of both the cryogenic and ambient SMAT processes can be found in [16]. Briefly, the material to be treated is fitted onto one end of the vial in a mechanical alloying mill (SPEX, Company, Metuchen, NJ, USA); the milling media within the vial, in this case 50 g of stainless steel shot, continually impacts the surface at high rate and variable direction during the SMAT process. For the cryogenic SMAT process, the milling vial is enclosed by a Teflon sleeve through which liquid nitrogen is continuously flowing throughout the treatment. The iron plates were polished to a mirror finish before treatment. The SMAT process was performed for one hour for both the ambient and cryogenic treatments.

Following the SMAT processes, the plates were sectioned and polished by a series of steps down to 1 μm alumina. The microstructural analysis was performed using an FEI Nova 600i dual beam (FEI, Hillsboro, OR, USA) Focused Ion Beam (FIB) system. Focused ion beam channeling contrast images (FIBCCI) are obtained using backscattered electrons produced by the ion beam as it rasters across the sample surface. The FIBCCI contrast mechanism is due to changes in the grain orientations that cause

variations in ion channeling efficiency, *i.e*., crystals which are able to channel more effectively due to their orientation produce fewer detectable electrons, so orientations closer to incident ions show up darker, *i.e*., crystal orientation specific contrast.

Hardness measurements were obtained with a Wilson Hardness Tukon 1202 (Buehler, Lake Bluff, IL, USA) using a load of 50 g load with 10 s dwell time with three measurements at each depth. Tensile test dogbones were cut from the SMAT plates with a MicroProtoSystems DSLS 3000 micromill (MicroProtoSystems, Chandler, AZ, USA) with the approximate gauge dimensions: 5 mm length, 1 mm width, and thickness of ~350 μm. The tensile tests were performed on a custom miniature tensile test apparatus which utilizes digital image correlation to track the sample extension. Three tensile tests for each sample were performed at a load rate of 2 μm/s with a 125 lb load cell.

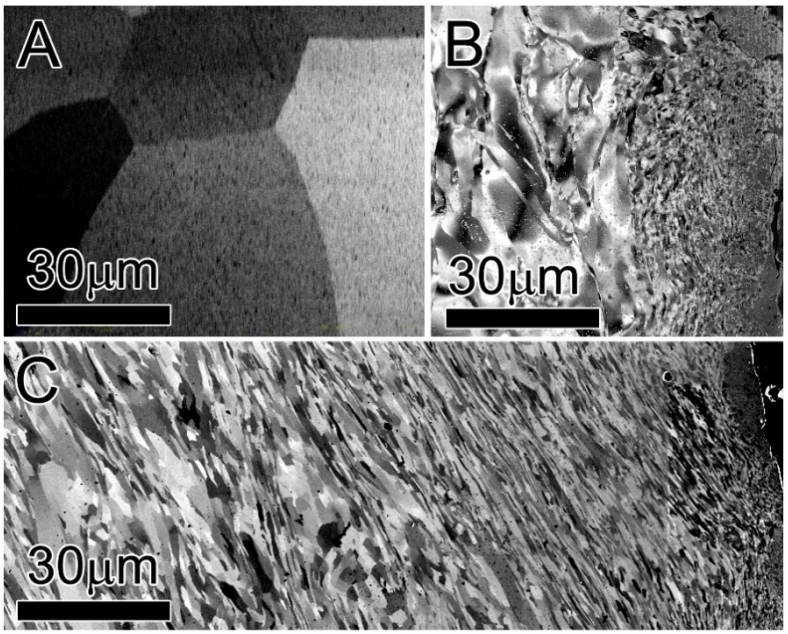

Figure 1. (**a**) Initial microstructure of the ARMCO Iron plate; (**b**) Surface microstructure following the cryogenic surface mechanical attrition treatment (SMAT), showing considerable grain refinement and plastic deformation; (**c**) Surface microstructure following ambient SMAT treatment. The grain refinement continues a considerable distance into the material.

3. Results and Discussion

3.1. Microstructure

The FIBCCI contrast micrograph (Figure 1A) reveals the initial grain size of the iron plate to be 50–100 μm. After the SMAT treatment at ambient temperature (Figure 1C), the plate exhibited submicron grains up to ~200 μm deep into the sample, with plastic deformation artifacts continuing up to about 700 μm. The average surface grain size (measured within the top 5 μm of the plate) was 650 nm. In contrast, the average surface grain size for the cryogenic SMAT treatment of the same duration was 350 nm (Figure 1C). As in the case of cryogenic SMAT copper, which showed a 60% reduction in grain size with respect to the ambient [16], the cryogenic SMAT iron followed the same

trend of higher grain refinement than the ambient SMAT treatment, but to a lesser extent. The reduction of grain size by only ~45% in the iron follows literature trends for microstructural refinement as described by the strain/temperature pairing through the Zener-Holloman parameter [18,22]. Iron has higher activation energy for deformation than copper, generally taken in pure metals as similar to the activation energy for self-diffusion; therefore, the grain refinement is less receptive to changes in temperature. In addition to the differences in surface grain size, the grain size gradient in the cryogenic SMAT iron is significantly sharper, exhibiting only a ~50 μm region of submicron grains and ~300 μm region of plastic deformation. The surface of the cryogenic SMAT iron also shows some surface cracks, as can be seen in the far upper right of Figure 1B.

3.2. Mechanical Properties

The microhardness as a function of depth into the plate is shown in Figure 2. The cryogenic SMAT sample had a higher surface hardness of 2.6 GPa compared to the ambient SMAT plate of 2.4 GPa, in line with predictions from the Hall-Petch relationship for iron [23]. The hardness of the cryogenic SMAT plate reduces more rapidly than in the ambient SMAT plate—dropping from 2.6 GPa to 2 GPa within the first 50 μm and then to ~1.7 GPa within the first 100 μm, mirroring the steepness of the gradient compared to the ambient cross sections. However, after the first ~100 μm, there is no significant difference in the hardness—as the grain size increases out of the ultrafinegrained regime, the variance in hardness with changes in grain size is minimal. Additionally, while the grain size grows rapidly in the cryogenic SMAT plate, the larger grains still contain a significant amount of deformation artifacts such as dislocation walls and tangles [17,24,25], as can be seen in the changing contrast in the channeling images. These microstructural features, internal to the grain boundaries, can also contribute to the observed hardness of the material.

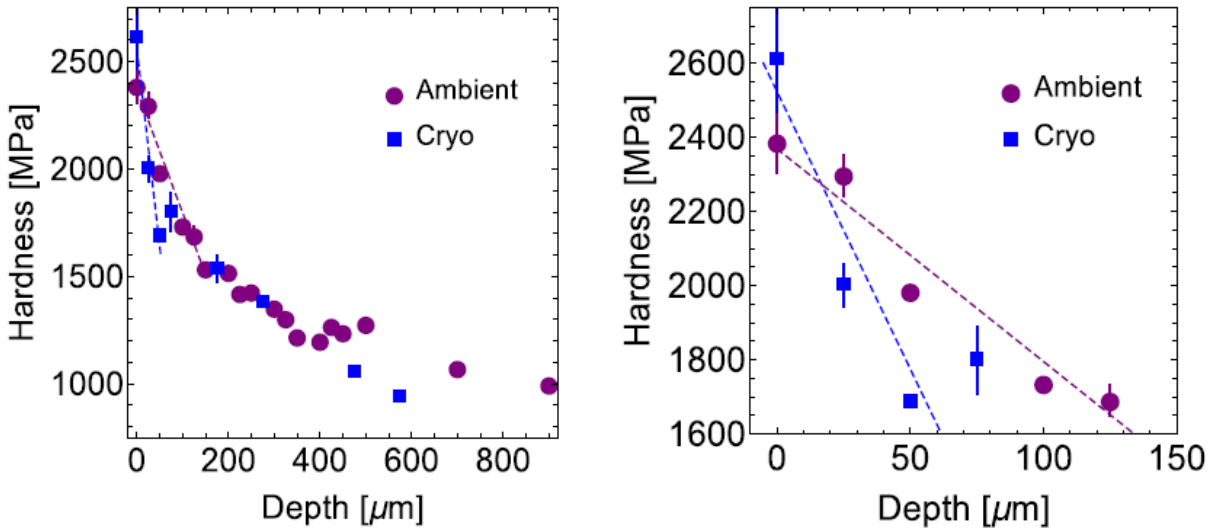

Figure 2. Microhardness of iron plates treated by the SMAT process as a function of depth into the sample. The values for the cryogenic SMAT iron are indicated by blue squares; ambient SMAT by purple circles. Dashed lines are a guide to the eye.

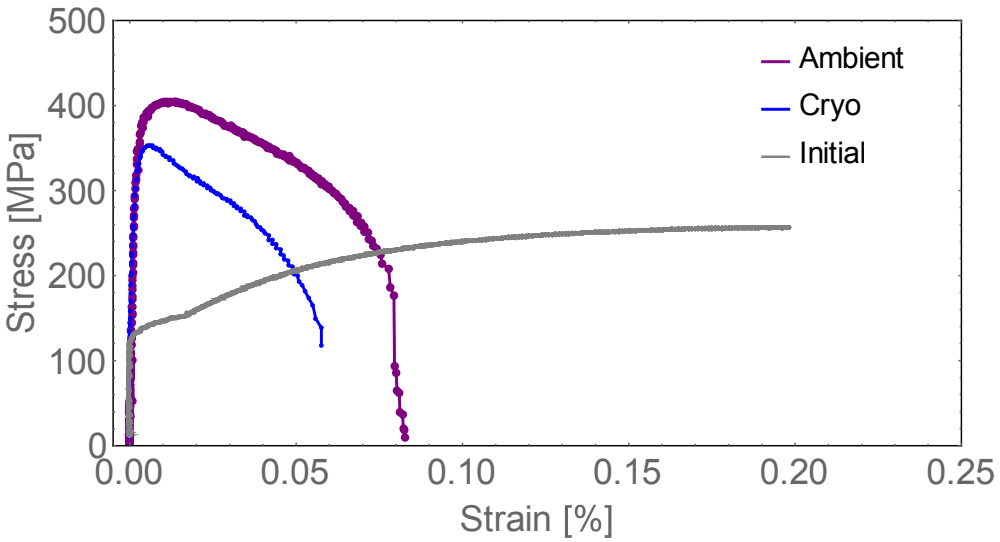

Figure 3. Tensile behavior for cryogenic SMAT (blue curve), ambient SMAT (purple curve) iron, and untreated iron plate (gray curve). The cryogenic SMAT exhibits lower strength and ductility than the ambient SMAT. Both SMAT treated plates show improvement in strength and decrease in ductility as compared to the untreated iron.

The yield strengths of the cryogenic and ambient SMAT iron samples were 345 and 385 MPa respectively, significantly higher than that of the untreated iron plate (~150 MPa), as seen in Figure 3. While the higher surface grain refinement in the cryogenic SMAT gradient led to a higher surface hardness commensurate with Hall-Petch behavior (Figure 2), the opposite relationship is observed in the tensile tests, with the ambient SMAT iron exhibiting a higher yield strength. The gradient structure in the cryogenic SMAT plate only exhibited significant grain refinement to a depth of about 50 μm, comprising about 14% of the tensile dogbone thickness. The ambient SMAT gradient penetrated much deeper into the plate, encompassing closer to 60% of the thickness of the tensile specimen. A greater volume fraction of the tensile specimen is then comprised of ultrafine grains in the ambient SMAT iron, resulting in a higher overall yield strength. A similar result was observed in tensile specimens composed of a gradient twin layers, wherein the depth of the gradient into the dogbone sample was found to correspond to the strength according to a rule of mixtures [26]. An additional contribution to the poor mechanical behavior in the cryogenic SMAT iron may be due to the difference in surface condition between the two processes. As can be seen in Figure 1B, the surface of the cryogenic SMAT plate can exhibit small cracks than are attributed to the expected brittle (*versus* ductile) behavior at the greatly reduced processing temperature.

Both the cryogenic and ambient SMAT iron displayed very little uniform elongation before exhibiting significant strain softening in contrast to the strain hardening behavior of the initial iron plate (Figure 3). Nanocrystalline bcc iron usually exhibits brittle fracture in tension, while strain softening is observed in ultrafinegrained iron [20,27,28] in grain sizes as large as 4 μm [29]. A stress drop (e.g., the amount of softening) of ~400 MPa from yield to failure has been observed in homogenous ultrafinegrained iron samples of similar grain size to that of the surface grains in this work [20,28–30]. The total elongation is also in line with homogenous ultrafinegrained iron produced through ECAP [20,28,30] while the overall strength is lower due to the increasing grain size of the gradient out of the ultrafinegrained regime.

In contrast to this observed strain softening behavior, it was reported in [25] that a grain size gradient structure in steel exhibited extraordinary strain hardening; additionally, a grain size gradient in copper displayed significant strain hardening and tensile elongation as well [5]. To examine these differences, we first look at the two literature reports of significant strain hardening in grain size gradients. In contrast to iron, nanocrystalline and ultrafine-grain copper can display some strain hardening behavior [31]. Additionally, in the case of the grain size gradient in [5], the significant plastic deformation is found to be dominated by mechanically driven grain growth throughout the grain size gradient during loading.

The strain hardening behavior in the steel grain size gradient was not found to be a result of mechanical grain growth [25]; the varying regions of the gradient structure were tested separately and together to reveal a synergistic effect between the gradient region and the undeformed core material. When the gradient structure was isolated (e.g., the top 120 μm of the sample was tested separately), it did not exhibit strain hardening behavior, rather strain softening, with a yield drop of almost 100 MPa and elongation of <10%. Significant strain hardening was observed only when the tensile sample thickness included both the gradient layer and a considerable fraction of the undeformed steel; the gradient layer represented about 12% of the tensile sample thickness [25]. Additionally, the hardening behavior was measured as a function of depth through hardness measurements that were performed after the tensile test. Hardening was only exhibited towards the back end of the gradient structure (as the gradient transition to the undeformed core), where the grain size was much greater than 1 μm.

In this work on grain size gradient iron, the thickness of the tensile test samples was ~350 μm which encompasses only the refined grain size gradient and heavily deformed regions, and none of the pristine non-deformed coarse-grained core. The low tensile ductility is therefore a result of this truncation of the gradient before reaching the undeformed core, the tensile behavior of both the cryogenic and ambient SMAT processed iron is in line with that of the stand-alone steel gradient layer in [25] which exhibited low elongation and a lack of strain hardening. Standalone tests of the gradient surface layer in copper were also consistent with this mechanical behavior [5,32].

While still exhibiting good ductility, the grain size gradient in Cu-Zn [33] does not improve upon the strength-ductility tradeoff in homogenous grain size materials as significantly as the copper [5] and steel [25] gradients. The grain refinement in the Cu-Zn study is not quantified, but most of the grain sizes in the gradient appear to be much larger than 1 μm; additionally, the hardness measurements indicate that the entire thickness of the tensile samples (600 μm) has been plastically deformed, preventing the unusual elongation and hardening behavior accessed by the studies including the undeformed core [5,25].

The standard strength-ductility tradeoff associated with grain refinement is shown in Figure 4—a typical boundary region is shown with the dashed curve drawn through data points for homogeneous grain structures of the same material as the gradient structures: pure iron [34] (gray circles), pure copper [31,35–40] (gray diamonds), steel [25] (gray triangles), and Cu-Zn alloys [33] (gray squares). These points are data from bulk samples of various homogeneous grain sizes and processing methods for comparison with the gradient grain structures of the sample material. The strength and elongation of the existing data for grain size gradient structures – this work in iron (magenta circles), Cu-Zn alloys (red squares), steel (black triangle), and copper (orange diamond) are plotted with respect to the bulk literature data. Only the gradient structures that include a significant fraction of non-deformed grains in the tensile specimen (copper [5] and steel [25]) are significantly off the tradeoff curve for their pure homogenous counterparts. This further supports the work of [25], which describes the unusual

synergistic effect of the deformed gradient layer and the coarse-grained core. The typical strain softening behavior in bcc iron and the lack of an undeformed core section in the tensile specimens in this work explain the relatively poor position on the frontier of the strength-ductility tradeoff for the cryogenic and ambient SMAT iron, as compared to the other three gradient systems.

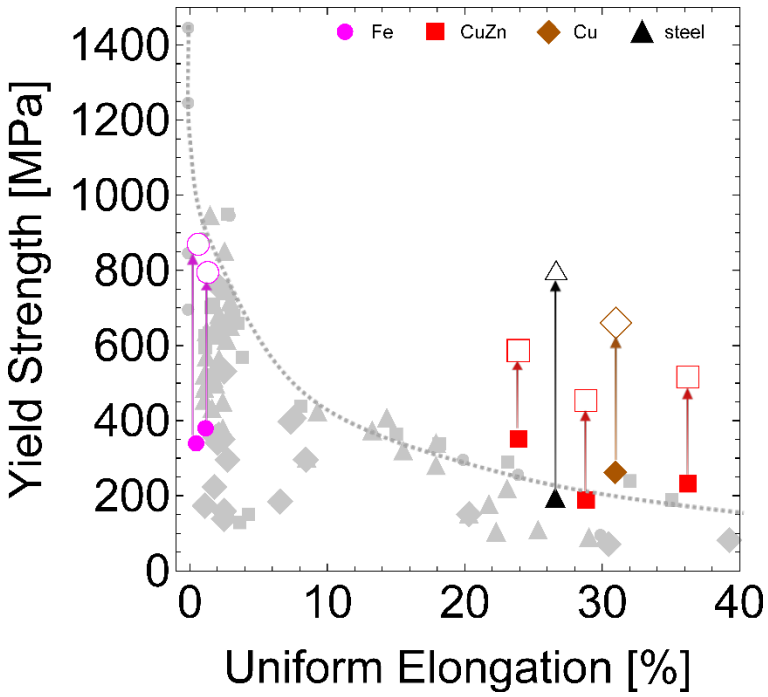

Figure 4. Tensile data existing for gradient grain structures are depicted for the iron SMAT in this work (magenta circles), Cu-Zn alloys [33] (red squares), copper [5] (orange diamond); steel [25] (black triangle). Literature values for bulk structures in the same materials are shown in gray (iron: gray circles [34], steel: grey triangles [25] and references therein, Cu-Zn alloys: grey squares [33] and references therein, copper: gray diamonds [31,35–40]). The strength ductility tradeoff is illustrated by the dotted line. The surface strength for each gradient structure is depicted with an open symbol of the same color and at the same elongation point, connected by a gradient arrow.

The surface strength of the grain size gradient structures is also plotted in Figure 4, at the sample elongation as the gradient material and marked with an open symbol of the same color. The surface yield strength shown is calculated from surface hardness measurements (yield ~ H/3) for the iron in this work, the Cu-Zn example, and the steel example; the surface yield strength for the pure copper example was from a tensile test of a free standing foil cut from the surface. In the work on steel [25], strength measurements reported from tensile tests performed with a foil cut from the surface layer and the hardness tests were congruent. While the overall strength and ductility of the gradient structure may not be a significant improvement on a bulk sample of a similar grain size, the surface strength is consistently a marked improvement over a homogenous grain size structure at the same elongation. This difference highlights an engineering advantage of grain size gradient materials, in that the surface of a grain size gradient structure can be as much as eight times harder than a homogenous grain size part of similar ductility.

4. Conclusions

The application of surface mechanical attrition treatment at both ambient and cryogenic temperatures to bcc iron plate resulted in significant surface grain refinement and resulted in a grain size gradient. The cryogenic SMAT produced a 45% greater grain size reduction as compared to the ambient SMAT, but a shallower depth of grain refinement. Consequently, the surface hardness was higher for the cryogenic SMAT, but the tensile strength and ductility was lower, due to the lower volume fraction of ultrafine-grains. Strain softening is observed, in line with iron with homogenous grain sizes in the ultrafine-grain regime. The tensile elongation of both grain size gradients remains low (<10%), in contrast to the extraordinary strain hardening observed in grain size gradient work in steel [25], due to the lack of undeformed core region in the tensile samples. Moving forward, the relationship between the volume fraction of gradient grains/deformed region and ductility should be explored in order to successfully exploit the benefits of nanocrystalline surface layers while maintaining ductility in the larger part.

Acknowledgments

The authors would like to acknowledge Jim Catalano (ARL), Tom Luckenbaugh (Bowhead) and Micah Gallagher (Bowhead) for valuable experimental input. AJR would like to acknowledge support from the U.S. Army Research Laboratory administered by the Oak Ridge Institute for Science and Education through an interagency agreement between the U.S. Department of Energy and ARL.

Author Contributions

H.A.M. and K.A.D. conceived and designed the experiments; A.J.R. and H.A.M performed the experiments; H.A.M. and K.A.D. analyzed the data; H.A.M. created the initial draft and all authors discussed the results, participated in the manuscript preparation, and approved the final manuscript.

Conflicts of Interest

The authors declare no conflict of interest.

References

1. Wang, Y.; Chen, M.; Zhou, F.; Ma, E. High tensile ductility in a nanostructured metal. *Nature* **2002**, *419*, 912–915.
2. Srinivasarao, B.; Oh-ishi, K.; Ohkubo, T.; Hono, K. Bimodally grained high-strength Fe fabricated by mechanical alloying and spark plasma sintering. *Acta Mater.* **2009**, *57*, 3277–3286.
3. Lu, L.; Chen, X.; Huang, X.; Lu, K. Revealing the maximum strength in nanotwinned copper. *Science* **2009**, *323*, 607–610.
4. You, Z.S.; Lu, L.; Lu, K. Tensile behavior of columnar grained Cu with preferentially oriented nanoscale twins. *Acta Mater.* **2011**, *59*, 6927–6937.
5. Fang, T.H.; Li, W.L.; Tao, N.R.; Lu, K. Revealing extraordinary intrinsic tensile plasticity in gradient nano-grained copper. *Science* **2011**, *331*, 1587–1590.

6. Balusamy, T.; Sankara Narayanan, T.S.N.; Ravichandran, K.; Park, I.S.; Lee, M.H. Influence of surface mechanical attrition treatment (SMAT) on the corrosion behaviour of aisi 304 stainless steel. *Corros. Sci.* **2013**, *74*, 332–344.
7. Fabijanic, D.; Taylor, A.; Ralston, K.D.; Zhang, M.X.; Birbilis, N. Influence of surface mechanical attrition treatment attrition media on the surface contamination and corrosion of magnesium. *Corrosion* **2012**, *69*, 527–535.
8. Huang, R.; Han, Y. The effect of smat-induced grain refinement and dislocations on the corrosion behavior of Ti–25Nb–3Mo–3Zr–2Sn alloy. *Mater. Sci. Eng C* **2013**, *33*, 2353–2359.
9. op't Hoog, C.; Birbilis, N.; Estrin, Y. Corrosion of pure Mg as a function of grain size and processing route. *Adv. Eng. Mater.* **2008**, *10*, 579–582.
10. Dai, K.; Shaw, L. Comparison between shot peening and surface nanocrystallization and hardening processes. *Mater. Sci. Eng. A* **2007**, *463*, 46–53.
11. Ortiz, A.L.; Tian, J.-W.; Shaw, L.L.; Liaw, P.K. Experimental study of the microstructure and stress state of shot peened and surface mechanical attrition treated nickel alloys. *Scr. Mater.* **2010**, *62*, 129–132.
12. Shaw, L.L.; Tian, J.-W.; Ortiz, A.L.; Dai, K.; Villegas, J.C.; Liaw, P.K.; Ren, R.; Klarstrom, D.L. A direct comparison in the fatigue resistance enhanced by surface severe plastic deformation and shot peening in a C-2000 superalloy. *Mater. Sci. Eng. A* **2010**, *527*, 986–994.
13. Villegas, J.C.; Shaw, L.L.; Dai, K.; Yuan, W.; Tian, J.; Liaw, P.K.; Klarstrom, D.L. Enhanced fatigue resistance of a nickel-based hastelloy induced by a surface nanocrystallization and hardening process. *Philos. Mag. Lett.* **2005**, *85*, 427–438.
14. Roland, T.; Retraint, D.; Lu, K.; Lu, J. Fatigue life improvement through surface nanostructuring of stainless steel by means of surface mechanical attrition treatment. *Scr. Mater.* **2006**, *54*, 1949–1954.
15. Efe, M.; El-Atwani, O.; Guo, Y.; Klenosky, D.R. Microstructure refinement of tungsten by surface deformation for irradiation damage resistance. *Scr. Mater.* **2014**, *70*, 31–34.
16. Darling, K.A.; Tschopp, M.A.; Roberts, A.J.; Ligda, J.P.; Kecskes, L.J. Enhancing grain refinement in polycrystalline materials using surface mechanical attrition treatment at cryogenic temperatures. *Scr. Mater.* **2013**, *69*, 461–464.
17. Tao, N.R.; Wang, Z.B.; Tong, W.P.; Sui, M.L.; Lu, J.; Lu, K. An investigation of surface nanocrystallization mechanism in Fe induced by surface mechanical attrition treatment. *Acta Mater.* **2002**, *50*, 4603–4616.
18. Li, Y.; Zhang, Y.; Tao, N.; Lu, K. Effect of the zener–hollomon parameter on the microstructures and mechanical properties of Cu subjected to plastic deformation. *Acta Mater.* **2009**, *57*, 761–772.
19. Pu, Z.; Song, G.L.; Yang, S.; Outeiro, J.C.; Dillon, O.W., Jr.; Puleo, D.A.; Jawahir, I.S. Grain refined and basal textured surface produced by burnishing for improved corrosion performance of AZ31B Mg alloy. *Corros. Sci.* **2012**, *57*, 192–201.
20. Han, B.; Mohamed, F.; Lavernia, E. Mechanical properties of iron processed by severe plastic deformation. *Metall. Mater. Trans. A* **2003**, *34*, 71–83.
21. Wei, Q. Strain rate effects in the ultrafine grain and nanocrystalline regimes-influence on some constitutive responses. *J. Mater. Sci.* **2007**, *42*, 1709–1727.
22. Vorhauer, A.; Pippan, R. On the onset of a steady state in body-centered cubic iron during severe plastic deformation at low homologous temperatures. *Metall. Mater. Trans. A* **2008**, *39*, 417–429.

23. Malow, T.R.; Koch, C.C. Mechanical properties, ductility, and grain size of nanocrystalline iron produced by mechanical attrition. *Metall. Mat. Trans. A* **1998**, *29*, 2285–2295.
24. Lu, K.; Lu, J. Nanostructured surface layer on metallic materials induced by surface mechanical attrition treatment. *Mater. Sci. Eng. A* **2004**, *375–377*, 38–45.
25. Wu, X.; Jiang, P.; Chen, L.; Yuan, F.; Zhu, Y.T. Extraordinary strain hardening by gradient structure. *Proc. Natl. Acad. Sci. USA* **2014**, *111*, 7197–7201.
26. Wang, H.T.; Tao, N.R.; Lu, K. Architectured surface layer with a gradient nanotwinned structure in a Fe–Mn austenitic steel. *Scr. Mater.* **2013**, *68*, 22–27.
27. Jia, D.; Ramesh, K.T.; Ma, E. Effects of nanocrystalline and ultrafine grain sizes on constitutive behavior and shear bands in iron. *Acta Mater.* **2003**, *51*, 3495–3509.
28. Bolaños, J.A.M.; Cobos, O.F.H.; Marrero, J.M.C. Strain hardening behavior of armco iron processed by ECAP. *IOP Conf. Ser. Mater. Sci. Eng.* **2014**, *63*, 012143.
29. Ding, Y.; Jiang, J.; Shan, A. Plastic instability and strain rate sensitivity of ultrafine-grained iron. *J. Alloys Compd.* **2009**, *487*, 517–521.
30. Takaki, S.; Kawasaki, K.; Futamura, Y.; Tsuchiyama, T. Deformation behavior of ultrafine grained iron. *Mater. Sci. Forum* **2006**, *503–504*, 317–322.
31. Legros, M.; Elliott, B.R.; Rittner, M.N.; Weertman, J.R.; Hemker, K.J. Microsample tensile testing of nanocrystalline metals. *Philos. Mag. A* **2000**, *80*, 1017–1026.
32. Ma, E. Instabilities and ductility of nanocrystalline and ultrafine-grained metals. *Scr. Mater.* **2003**, *49*, 663–668.
33. Cai, B.; Ma, X.; Moering, J.; Zhou, H.; Yang, X.; Zhu, X. Enhanced mechanical properties in Cu–Zn alloys with a gradient structure by surface mechanical attrition treatment at cryogenic temperature. *Mater. Sci. Eng. A* **2015**, *626*, 144–149.
34. Cheng, S.; Milligan, W.W.; Wang, X.L.; Choo, H.; Liaw, P.K. Compressive and tensile deformation behavior of consolidated Fe. *Mater. Sci. Eng. A* **2008**, *493*, 226–231.
35. Wang, Y.M.; Wang, K.; Pan, D.; Lu, K.; Hemker, K.J.; Ma, E. Microsample tensile testing of nanocrystalline copper. *Scr. Mater.* **2003**, *48*, 1581–1586.
36. Nieman, G.W.; Weertman, J.R.; Siegel, R.W. Mechanical behavior of nanocrystalline metals. *Nanostructured Mater.* **1992**, *1*, 185–190.
37. Gertsman, V.Y.; Valiev, R.Z.; Akhmadeev, N.A.; Mishin, O.V. Deformation behavior of ultrafine-grained materials. *Mater. Sci. Forum* **1996**, *225–227*, 739–744.
38. Sanders, P.G.; Eastman, J.A.; Weertman, J.R. Elastic and tensile behavior of nanocrystalline copper and palladium. *Acta Mater.* **1997**, *45*, 4019–4025.
39. Lu, L.; Wang, L.B.; Ding, B.Z.; Lu, K. High-tensile ductility in nanocrystalline copper. *J. Mater. Res.* **2000**, *15*, 270–273.
40. Valiev, R.Z.; Kozlov, E.V.; Ivanov, Y.F.; Lian, J.; Nazarov, A.A.; Baudelet, B. Deformation behaviour of ultra-fine-grained copper. *Acta Metall. Mater.* **1994**, *42*, 2467–2475.